Aging Brain 5 (2024) 100110

Contents lists available at ScienceDirect

Aging Brain

journal homepage: www.elsevier.com/locate/nbas

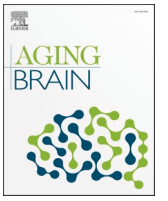

Targeted brain-specific tauopathy compromises peripheral skeletal muscle integrity and function

Bryan Alava [a,b], Gabriela Hery [b], Silvana Sidhom [a], Miguel Gutierrez-Monreal [a], Stefan Prokop [b,d], Karyn A. Esser [a], Jose Abisambra [b,c,e,*]

[a] Department of Physiology and Aging, University of Florida, Gainesville, FL 32610, USA
[b] Center for Translational Research in Neurodegenerative Disease (CTRND), University of Florida, Gainesville, FL 32610, USA
[c] Department of Neuroscience, University of Florida, Gainesville, FL 32610, USA
[d] Department of Pathology, University of Florida, Gainesville, FL 32610, USA
[e] Brain Injury Rehabilitation and Neuroresilience (BRAIN) Center, University of Florida, Gainesville, FL 32601, USA

A B S T R A C T

Tauopathies are neurodegenerative disorders in which the pathological intracellular aggregation of the protein tau causes cognitive deficits. Additionally, clinical studies report muscle weakness in populations with tauopathy. However, whether neuronal pathological tau species confer muscle weakness, and whether skeletal muscle maintains contractile capacity in primary tauopathy remains unknown. Here, we identified skeletal muscle abnormalities in a mouse model of primary tauopathy, expressing human mutant P301L-tau using adeno-associated virus serotype 8 (AAV8). AAV8-P301L mice showed grip strength deficits, hyperactivity, and abnormal histological features of skeletal muscle. Additionally, spatially resolved gene expression of muscle cross sections were altered in AAV8-P301L myofibers. Transcriptional changes showed alterations of genes encoding sarcomeric proteins, proposing a weakness phenotype. Strikingly, specific force of the soleus muscle was blunted in AAV8-P301L tau male mice. Our findings suggest tauopathy has peripheral consequences in skeletal muscle that contribute to weakness in tauopathy.

Introduction

Tauopathies, including Alzheimer's disease (AD) and frontotemporal dementias associated with chromosome 17 (FTD), are more than 20 neurodegenerative disorders that pathologically feature intracellular aggregates of the protein tau termed neurofibrillary tangles (NFTs) [1–5]. Tau canonically binds and stabilizes microtubules [5–7]; however, pathogenic processes disrupt tau-microtubule complexes. Emerging data characterizing tau interactomes suggest that tau performs functions beyond stabilizing microtubules, and therefore, alternative mechanisms may mediate tau pathogenic processes [8–16].

Besides cognitive decline, muscle weakness also manifests early in tauopathies. Patients with tauopathy can experience muscle weakness, sarcopenia, and frailty [17–19]. Moreover, murine models exhibiting AD-related amyloid pathology in the brain or targeted to skeletal muscle [20–21] show changes in skeletal muscle features such as specific force, fiber size, and muscle gene expression. These data link muscle weakness with AD, a tauopathy with amyloid plaque co-pathology, but it is not yet understood to what extent primary tau pathology independently impacts skeletal muscle. To explore the association between muscle weakness and onset of tau pathology, we investigated whether pathological tau species in the brain link to skeletal muscle abnormalities in a model of primary tauopathy.

Murine models, such as the JNPL3, PS19, and rTg4510 [22–27] models manifest motor deficits and muscle anomalies. However,

* Corresponding authors at: Center for Translational Research in Neurodegenerative Disease (CTRND), University of Florida, Gainesville, FL 32610, USA.
E-mail address: j.abisambra@ufl.edu (J. Abisambra).

https://doi.org/10.1016/j.nbas.2024.100110
Received 16 January 2024; Received in revised form 16 February 2024; Accepted 21 February 2024

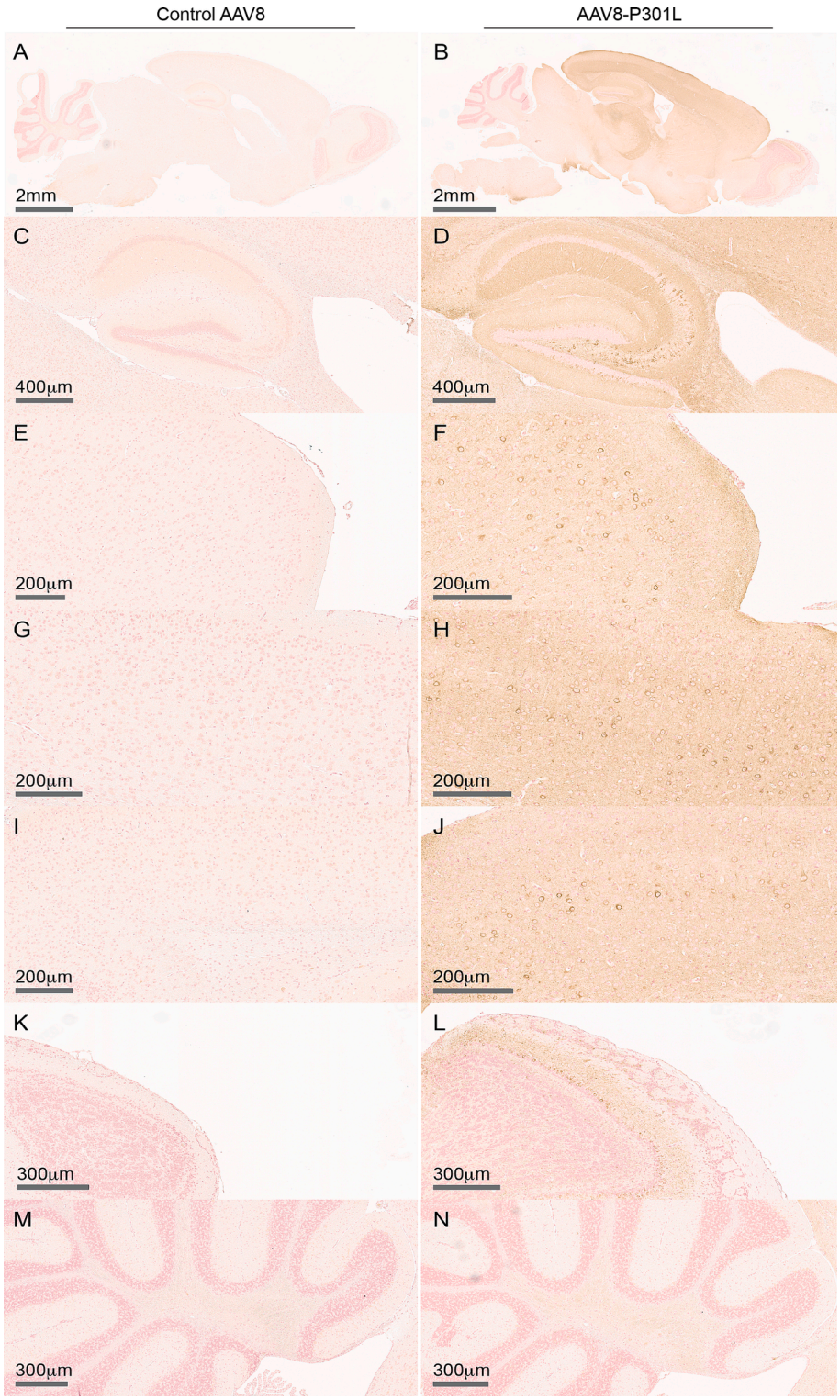

Fig. 1. AAV8-P301L tau expresses and deposits tau inclusions throughout the brain. Representative images of mouse brains stained with human tau antibody HT7. Compared to AAV8 control-injected mice (A,C,E,G,I,K,M), P301L-tau was detected in AAV8-P301L tau mouse brains (B). Human tau was largely detected in AAV8-P301L tau-expressing hippocampal, anterior, middle, and posterior cortical regions (D,F,H,J), and the olfactory bulb (L). The cerebellum showed limited P301L-tau immunoreactivity (N). N = 4 female, 7 male AAV8-P301L mice, N = 5 female, 6 male control AAV8 mice. See also Figure S1.

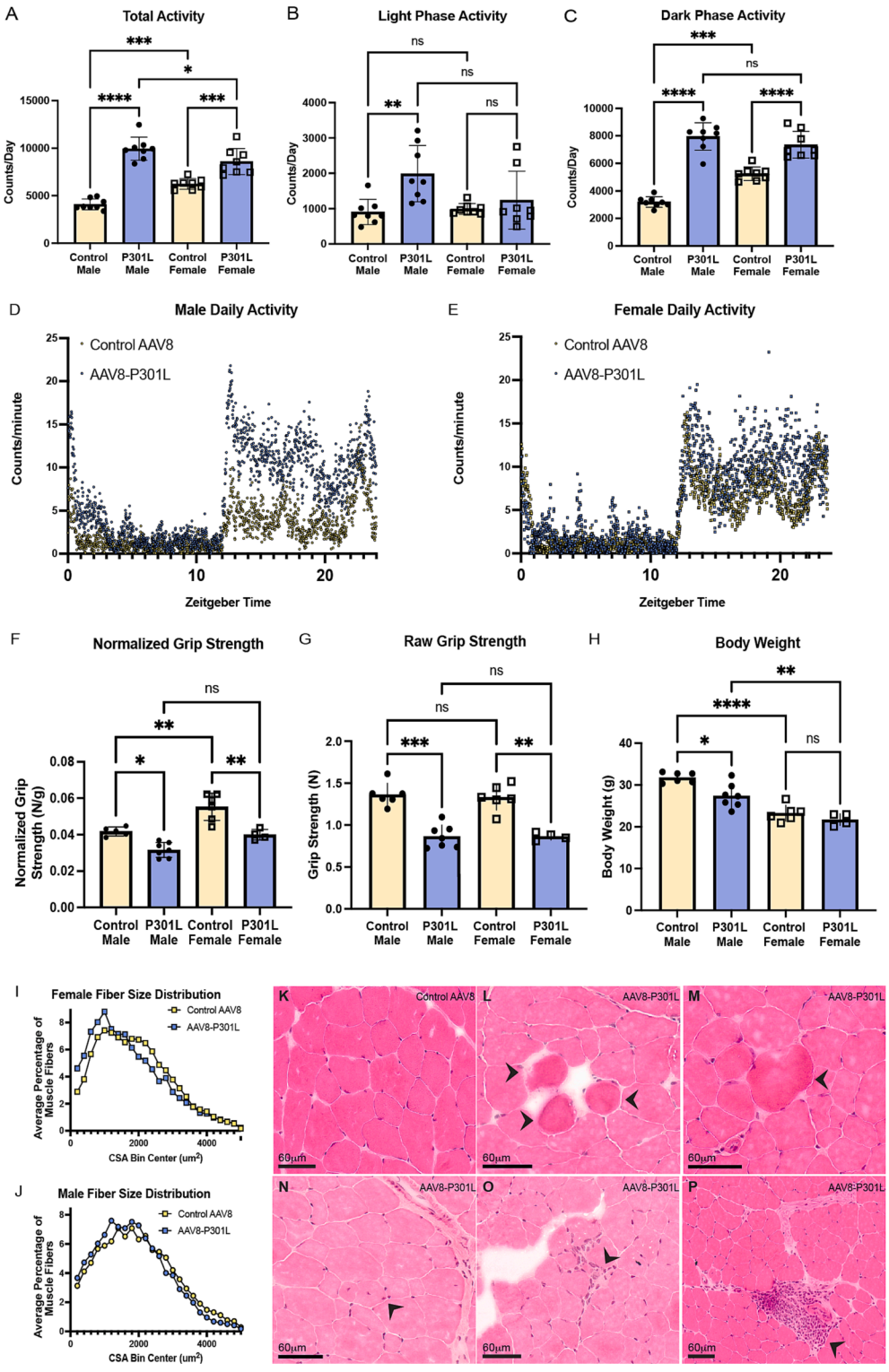

(caption on next page)

Fig. 2. Abnormal locomotor phenotypes and histological features persist in AAV8-P301L tau mice independent of changes in fiber size. A-E) AAV8-P301L tau mice are more active (A). Only male AAV8-P301L tau mice are more active in the light/rest phase compared to controls (B). Both male and female AAV8-P301L tau mice are more active in the dark/active phase compared to their sex matched controls (C). Averaged counts per minute for 7 days show increases in activity and no changes in timing of activity (D, E). N = 4 female, 7 male AAV8-P301L mice, N = 5 female, 6 male control AAV8 mice; Ordinary two-way ANOVA, *$p < 0.05$, ** $p < 0.01$, *** $p < 0.001$, *** $p < 0.0001$. See also Figure S2. F-H) Grip strength normalized to body weight is significantly reduced in AAV8-P301L male and female mice compared to their respective controls (F). Raw grip strength is reduced in the AAV8-P301L tau mice (G). Body weight was only significantly reduced in P301L tau expressing males (H). N = 4 female, 7 male AAV8-P301L mice, N = 5 female, 6 male control AAV8 mice; Ordinary two-way ANOVA, * $p < 0.05$, ** $p < 0.01$, *** $p < 0.001$. I-J) Calculated cross-sectional area distribution is unchanged in AAV8-P301L mice compared their sex-matched controls (I, J). N = 4 female, 5 male AAV8-P301L mice, N = 6 female, 6 male control AAV8 mice. See also Figure S2. K-P) Compared to wildtype mice (K), AAV8-P301L tau mice displayed subtle abnormalities in fiber shape and structure (circular fibers (L,M), group of smaller myofibers with central nuclei (N)) and abnormal clusters of nuclei ranging in severity (potentially pathogenic (O), and noticeably severe (P)).

whether these peripheral abnormalities are the consequence of brain-specific overexpression of pathological tau species, and whether muscle is impacted by tauopathy independent of peripheral nerve function, remains unknown. In this study, we performed an extensive evaluation of muscle structure and function in AAV8-P301L tau expressing mice. We found skeletal muscle abnormalities with the potential to induce physiological consequences, implicating skeletal muscle pathology and dysfunction as a peripheral symptom of tauopathy.

Results

Intraventricular AAV8-P301L tau expression promotes widespread pathology

We first validated that the PND0 intracerebroventricular brain injections of P301L tau induced tauopathy by harvesting 15-month-old AAV8-P301L tau-injected mouse brains (Fig. 1). Using a tau antibody that specifically recognizes human tau (HT7), we identified widespread and consistent human tau expression, which aligned with previously published data using ICV injections of AAV1-P301L tau [1]. Distribution was largely concentrated in the hippocampus, cortex (including the motor cortex), and olfactory bulb (Fig. 1), as expected. Limited immunoreactivity was observed in the cerebellum, suggesting fine motor control directed by the cerebellum may not be directly impacted by AAV8-guided P301L tau expression in this model. We also assessed accumulation of insoluble tau using biochemical analyses of soluble and sarkosyl-insoluble cortical tau. We identified increased immunoreactivity to pathology-associated pS202/T205 tau (AT8) in cortical samples of AAV8-P301L mice (Supplementary Fig. 1A, E, H). As expected, total tau (endogenous murine and AAV8-driven human) was also increased in AAV8-P301L mice (Supplementary Fig. 3B and G). We identified accumulation of soluble (Supplementary Fig. 1C, F) and sarkosyl-insoluble human-derived tau in cortical samples from the P3 pellet fraction (Supplementary Fig. 1D). These data provide histological and biochemical evidence that AAV8-P301L tau injected mice present neuropathological brain features of tauopathy.

AAV8-P301L tau expression promotes abnormal locomotor phenotypes and muscle histological features independent of changes in fiber size

AAV8-P301L tau mice showed increased daily cage activity compared to sex-matched controls at 8 months of age (Fig. 2a) as measured by infrared (IR) cage sensors. This increase is largely driven by activity during the dark/active phase; interestingly, male AAV8-P301L tau mice increased cage activity in both the light/inactive and dark/active phases (Fig. 2B-C). Activity in AAV8-P301L tau mice remained consistently increased each day during the 8-day recording period (Supplementary Fig. 2A–C), yet the timing of activity onset was not altered (Fig. 2D-E).

To determine changes in skeletal muscle due to tauopathy, grip strength was measured at 3 months of age, which is 3 months prior to the appearance of cognitive deficits previously established in this model [1]. P301L tau mice of both sexes showed grip strength deficits (Fig. 1F, G). The deficit in grip strength normalized to body weight (Fig. 2F) is driven largely by a reduction in raw grip strength, which was reduced in AAV8-P301L tau mice of both sexes (Fig. 2G). Surprisingly, body weight was significantly reduced in AAV8-P301L tau-expressing males but not females (Fig. 2H). These data suggest that this model manifests muscle weakness independently of their body weight.

To assess if general weakness was driven by changes in muscle size, we measured fiber size distribution of the tibialis anterior muscle. We did not observe differences in myofiber calculated cross-sectional area distribution (Fig. 2I, J) or minimum feret diameter distribution (Supplementary Fig. 2D, E). Therefore, altered fiber size distribution does not explain the grip strength weakness observed in this model.

We then assessed gross histological morphology of the tibialis anterior fibers. As expected, muscle sections from AAV8-P301L mice did not show visible signs of myofiber atrophy. Despite minor artifacts from freeze damage, there were common abnormalities in the tibialis anterior muscle of AAV8-P301L tau expressing mice not detected in the control mouse muscles. AAV8-P301L tau mice showed histological signs of myopathy, including circular fibers that deviated from normal polygonal shape (Fig. 2L, M) and relatively small fibers with central nuclei (Fig. 2 N). Darker, circular fibers were detected in 5 of the 8 mice, but not apparent in any controls. The most overt histological feature was the abnormal clustering of nuclei. The abnormal clustering ranged in severity in the cross sections between AAV8-P301L tau expressing mice. The majority of the AAV8-P301L tau mice displayed no nuclear clustering (4 out of the 8 AAV8-P301L mice), consistent with normal muscle (Fig. 2 K). However, nuclear clustering was seen in 3 out of the 8 AAV8-P301L tau

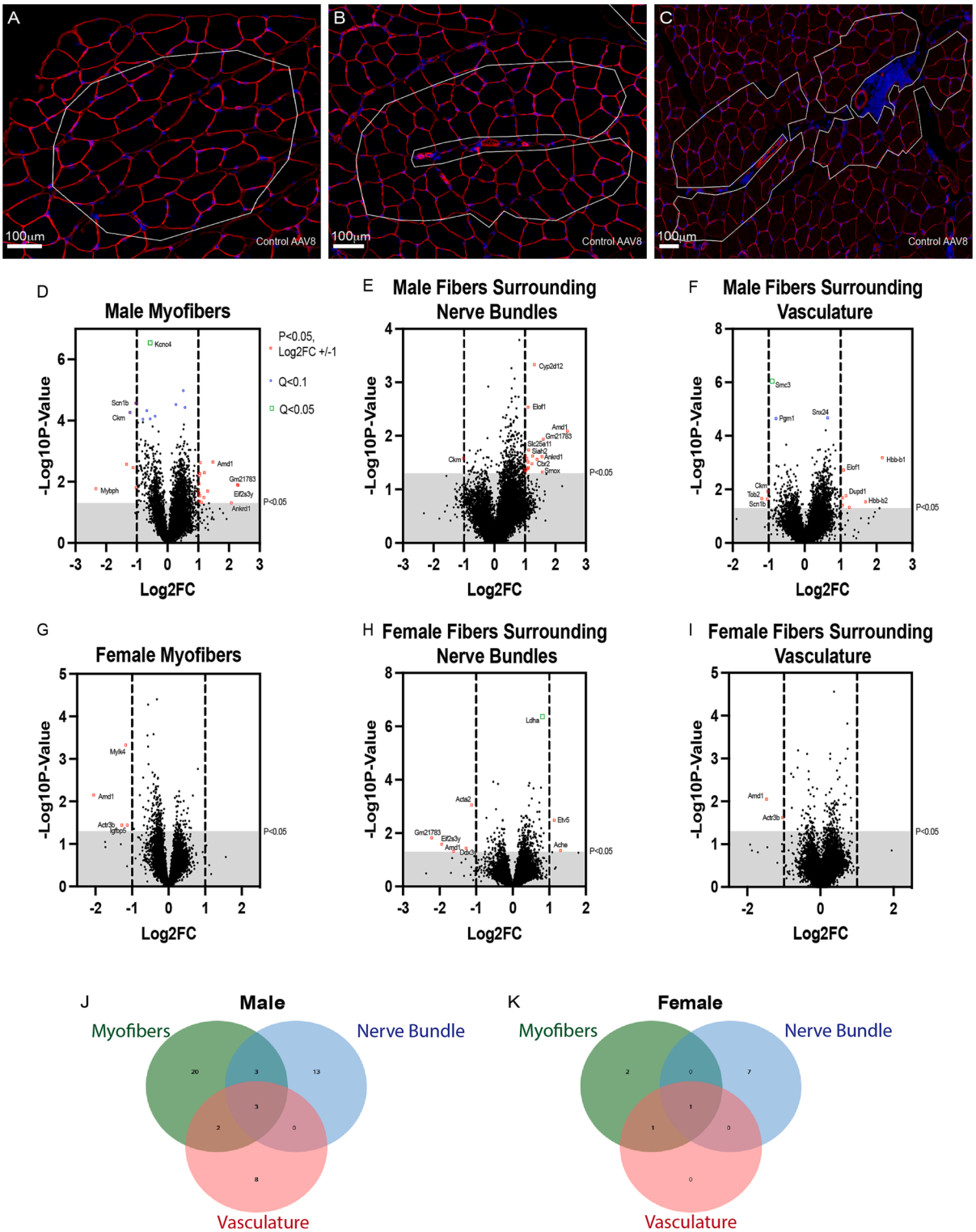

Fig. 3. Transcriptional differences in the tibialis anterior cross sections of AAV8-P301L tau mice are sex and muscle hallmark proximity dependent. Representative images of standard myofiber regions (without central nuclei and not directly proximal to a nerve bundle or vasculature) (A), regions of myofibers proximal to nerve bundles (B), and proximal to blood vessels (C showing two regions). Differentially detected transcripts for each sex and region type annotated by $Q < 0.05$ (Green), $Q < 0.1$ (Blue), or $P_{unadj} < 0.05$ and Log2FC +/-1 (Red)(D-I). Region-type and sex specificity of differentially detected transcripts (J, K). Linear Mixed Model with Benjamini-Hochberg correction for Q values. N = 3 mice/sex/treatment. 2 replicates per region type per mouse. Red: laminin stain; Blue: SYTO-13 stain. See also Figure S3.

Table 1
DEGs in AAV8-P301L tau expressing mice.

Male Myofibers			
Target name	Log2FC	Pvalue	Adjusted pvalue
Ckm	−1.223424	5.42E-05	0.08388866
Scn1b	−1.0300532	2.70E-05	0.08100621
Kcnc4	−0.5696607	2.88E-07	0.00312568
Slc25a11	0.510723	1.06E-05	0.05723474
Slc23a1	0.5654211	3.74E-05	0.08100621
Ywhae	−0.6794759	4.71E-05	0.08388866
Eif4g3	−0.4080474	7.21E-05	0.0977194
Naca	−0.5668857	8.74E-05	0.0977194
Stat5b	−0.8005968	9.01E-05	0.0977194
Mybph	−2.3325435	0.01700532	0.38690249
Myh4	−1.3307133	0.00266938	0.28691265
Tob2	−1.1200037	0.0034837	0.28691265
Atp1b2	−1.0229426	0.01553616	0.37699205
Tmem37	1.0035063	0.01968001	0.39586398
Evc	1.0252084	0.01164528	0.37151128
Acp2	1.028245	0.0237553	0.41878849
Ddx3y	1.0394324	0.04314541	0.48795466
Cyp2d12	1.0444787	0.00618857	0.31719049
Cbarp	1.0453949	0.0285243	0.43973768
Elof1	1.0497791	0.00537064	0.30146151
Actr3b	1.0683352	0.00235713	0.28395515
Egfl7	1.109266	0.04697204	0.49777939
Casq2	1.1814007	0.03262398	0.45817246
Ggt6	1.1996301	0.00500091	0.30146151
Smim22	1.3061328	0.0201995	0.39759725
Amd1	1.4749252	0.00224802	0.28395515
Ankrd1	2.0771373	0.04901014	0.5006879
Eif2s3y	2.2741486	0.01247633	0.37296408
Female Myofibers			
Target name	Log2FC	Pvalue	Adjusted pvalue
Igfbp5	−1.1322129	0.03614696	0.99970743
Actr3b	−1.2821699	0.03614657	0.99970743
Amd1	−2.0494655	0.00702363	0.99970743
Mylk4	−1.1727313	0.00047105	0.92529918
Male Regions Surrounding Nerve Bundles			
Target name	Log2FC	Pvalue	Adjusted pvalue
Ms4a4c	1.10149925	0.03088168	0.77313226
St8sia1	1.0088968	0.04866799	0.77313226
Elof1	1.10484112	0.00291215	0.77313226
Slc25a47	1.23161827	0.03333062	0.77313226
Prdx6	1.04290911	0.0432383	0.77313226
Cbr2	1.39834189	0.0275158	0.77313226
Rasd2	1.25242516	0.02362968	0.77313226
Rgs19	1.01618314	0.04309642	0.77313226
Slc25a11	1.01352213	0.02397385	0.77313226
Cyp2d12	1.31151068	0.00046528	0.77313226
Rspo3	1.1106034	0.03912526	0.77313226
Ckm	−1.0185573	0.02620283	0.77313226
Siah2	1.12064573	0.01821815	0.77313226
Saa1	1.0889167	0.04102098	0.77313226
Gm21783	1.60494891	0.01151605	0.77313226
Slamf9	1.06905824	0.02668728	0.77313226
Amd1	2.39189469	0.00813251	0.77313226
Ankrd1	1.5641015	0.02454313	0.77313226
Smox	1.57293036	0.04718639	0.77313226
Female Regions Surrounding Nerve Bundles			
Target name	Log2FC	Pvalue	Adjusted pvalue
Ldha	0.81662798	4.33E-07	0.00469031
Acta2	−1.1253701	0.00088288	0.91251361
Etv5	1.13598961	0.00326753	0.99823885
Gm21783	−2.2184757	0.01492758	0.99823885
Amd1	−1.2783677	0.03673931	0.99823885

(*continued on next page*)

Table 1 (*continued*)

Male Myofibers			
Target name	Log2FC	Pvalue	Adjusted pvalue
Eif2s3y	−1.9431755	0.02613885	0.99823885
Ache	1.30814964	0.04506988	0.99823885
Ddx3y	−1.6179833	0.0482479	0.99823885
Male Regions Surrounding Vasculature			
Target name	Log2FC	Pvalue	Adjusted pvalue
Smc3	−0.9036815	9.11E-07	0.00987269
Snx24	0.64237761	2.09E-05	0.08084234
Pgm1	−0.7949545	2.24E-05	0.08084234
Tob2	−1.0268414	0.01175089	0.57819522
1700001O22Rik	1.24247914	0.04655908	0.68686433
Elof1	1.08407078	0.00188693	0.45494996
Scn1b	−1.1927629	0.02174677	0.61217135
Cyp2d12	1.06012617	0.02053396	0.60623039
Ckm	−1.0382894	0.023112	0.61826787
Hbb-b1	2.16156834	0.00065385	0.41950071
Hbb-b2	1.69329888	0.02884086	0.64474412
Dyrk2	1.0546524	0.03909395	0.66854108
Dupd1	1.15233126	0.01712163	0.60480048
Female Regions Surrounding Vasculature			
Target name	Log2FC	Pvalue	Adjusted pvalue
Actr3b	−1.0293919	0.02382635	0.94802223
Amd1	−1.4728549	0.0088693	0.94802223

muscles analyzed (Fig. 2O), and severe nuclei grouping was observed in 1 AAV8-P301L tau muscle cross section (Fig. 2P). The severe nuclei grouping was apparent in the three serial cross sections analyzed. There was not a correlation with degree of soluble or insoluble tau biochemical detection and presence/absence of histological findings. Since cross sections are representative of only the sagittal view of the fibers, there may be additional pathogenic features in the muscle of other mice not captured in the cross sections analyzed. Therefore, distinctions in AAV8-P301L myofibers observed with H&E analysis was strengthened with a spatial transcriptomic study.

Altered transcript detection in the tibialis anterior of AAV8-P301L tau expressing mice is sex and region specific

To determine if selected regions of myofibers from AAV8-P301L tau-expressing mice were distinct from controls, spatial transcriptomics was performed on cross sections of the tibialis anterior muscle of AAV8-P301L tau mice and AAV8 controls. To compare the localized gene expression patterns, we selected regions of visually normal myofibers, myofibers proximal to vasculature, and myofibers proximal to nerve bundles (Fig. 3A-C). These regions were selected to reflect potential sites of communication from the central nervous system to the muscle. To visualize the regions, we stained the muscle cross sections with laminin and SYTO-13 (Supplementary Fig. 3) and selected regions that were in proximity to the section landmarks noted above.

We detected altered gene expression in visually normal myofiber regions in AAV8-P301L mice (Fig. 3 and Table 1). Twenty-eight differentially expressed genes (DEGs) were identified in AAV8-P301L males and 4 in AAV8-P301L females (Fig. 3D, G). Creatine Kinase (*Ckm)*, an important metabolic enzyme that supports high energy levels of phosphocreatine in skeletal muscle was surprisingly downregulated in AAV8-P301L males. DEGs encoding sarcomeric proteins such as *Mybph* (Myosin Binding Protein H, downregulated), *Myh4* (Myosin Heavy Chain 2B/fast, downregulated), and *Ankrd1* (Ankyrin Repeat Domain-Containing Protein 1, upregulated) were identified in males, and *Mylk4* (Myosin Light Chain Kinase Family Member 4) was downregulated in females. Beyond sarcomeric proteins, the transcript for calcium sequestering protein 2 (*Casq2 cardiac/slow muscle)* was also upregulated in males. This would increase the calcium buffering capacity in the muscle of the AAV8-P301L muscle. Moreover, the *Scn1b* (Sodium Voltage-Gated Channel Beta Subunit 1) transcript was downregulated in AAV8-P301L males. This encodes a regulatory subunit of the voltage-gated sodium channel, which is essential for action potential initiation and propagation.

Increased quantity of DEGs was also observed in AAV8-P301L males compared to females in regions of myofibers surrounding nerve bundles (19 vs 8 DEGs) (Fig. 3E, H). Reduced *Ckm* was evident in this region in AAV8-P301L males as was noted earlier. The detection of the *Ankrd1* transcript was upregulated in males, reflecting what was detected in visually normal myofibers. Interestingly, *Ache* (Acetylcholinesterase) was upregulated in female regions surrounding nerve bundles. Acetylcholinesterase functions in the rapid degradation of synaptic acetylcholine at the neuromuscular junction. Therefore, its upregulation would be consistent with more rapid clearing of acetylcholine at the neuromuscular junction. Since *Ache* expression is spatially detected in muscle fibers at the neuromuscular junction, it is important to note that AAV8-P301L muscle gene expression for all subunits of the acetylchline receptor were unchanged in these regions. Therefore, in normal conditions, a change in *Ache* expression is not expected in these regions.

We identified the same sex-specific distinctions (increased DEGs in males) reflected in myofibers located proximal to blood vessels (Fig. 3F, I). Thirteen DEGs were present in AAV8-P301L males, and only 2 in females. We observed downregulation of *Ckm* and *Scn1b*

in males, resembling the visually normal myofibers.

Interestingly, *Amd1* (adenosylmethionine decarboxylase 1, polyamine biosynthesis) was differentially detected in 5 of the 6 region types analyzed. *Amd1* was consistently downregulated in females, and consistently upregulated males. Sex specificity to polyamine biosynthesis has been described and may explain this observation [28]. Most differentially detected transcripts had regional specificity that was determined by sex (Figs. 3J, K). However, many differentially detected transcripts encoded proteins present at the sarcomere or essential for generating force, and they were detected in every region for both sexes (Table 1).

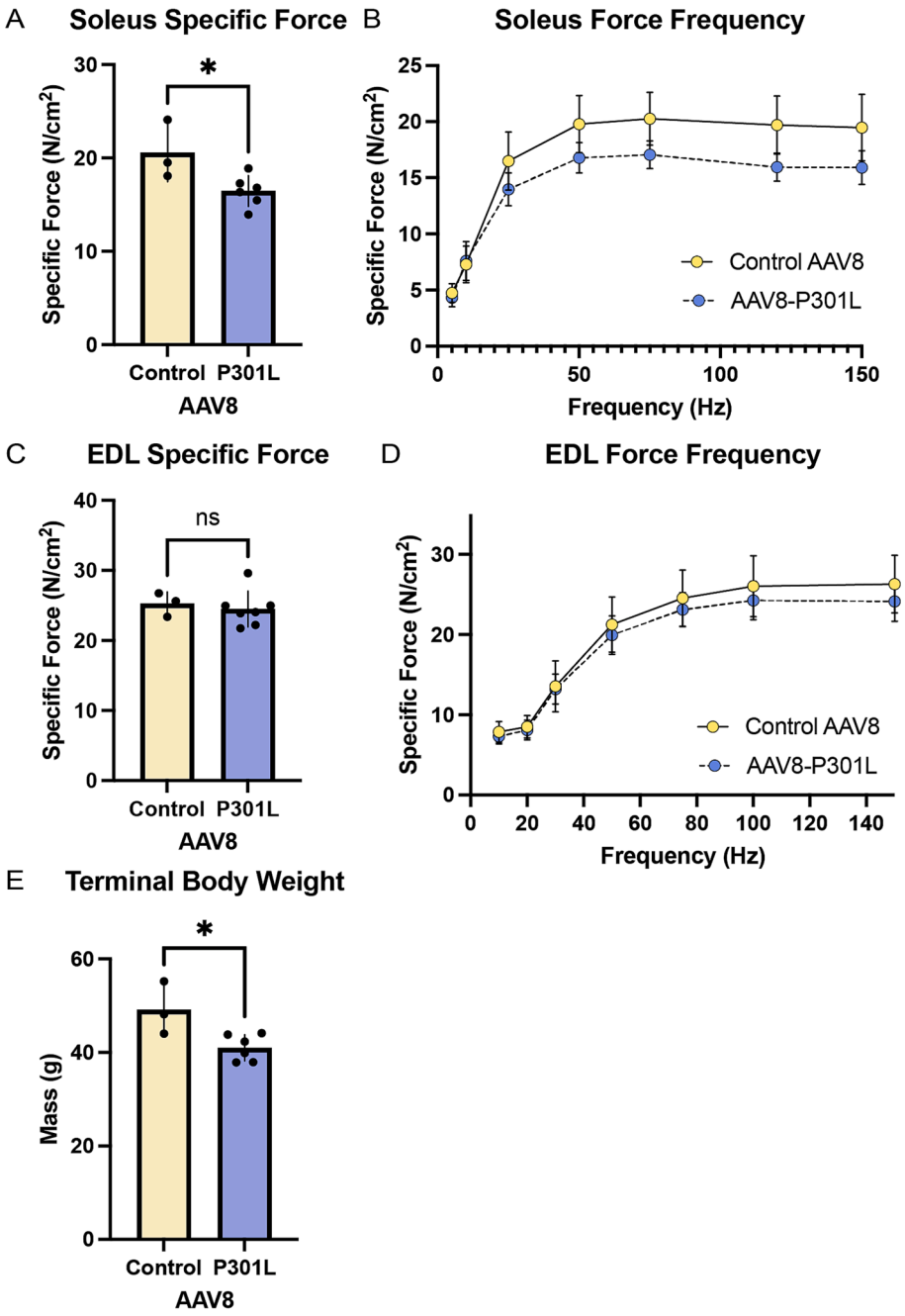

Fig. 4. Ex vivo specific force of the soleus is reduced in AAV8-P301L tau expressing males. Soleus *ex vivo* specific force calculations are reduced in the AAV8-P301L tau expressing males (A), and normal force frequency curves are observed (B). Specific force of the EDL muscle is sustained (C-D). Reduced body weight was maintained in AAV8-P301L male mice at time of collection (E). N = 6–7 male AAV8-P301L tau mice, N = 3 control AAV8 male mice; Student's *t*-test, *P $<$ 0.05. See also Figure S4.

Reduction of specific force in the muscle of AAV8-P301L tau male mice

We hypothesized that changes in the levels of transcripts encoding sarcomeric proteins alter force generation in AAV8-P301L tau expressing mice, and that these changes were independent of neuronal signaling. To determine whether limited contractile force production contributes to weakness in AAV8-P301L tau mice, we obtained *ex vivo* measures of maximum isometric tetanic force from two different muscles in the hindlimb: the soleus muscle and the extensor digitorum longus (EDL) muscle. Given that changes in cage activity and DEG were more pronounced in male mice, we focused primarily in males. *Ex vivo* muscle mechanical measures activate the muscle using field stimulation and reflect the intrinsic force generating capacity of the muscle, which is not indicative of nerve-muscle communication. Therefore, the data acquired with this technique reflects changes in muscle phenotype independently from potential changes in the motor neuron or neuromuscular junction. Specific force, which is maximum isometric tetanic force normalized to muscle size (physiological cross-sectional area) was significantly reduced in the soleus of AAV8-P301L tau males compared to controls (Fig. 4A). This finding demonstrates that intrinsic force generating properties of the soleus, an important postural muscle, are impaired in this tauopathy model. Analysis of the soleus force-frequency properties did not detect shifts between the control and AAV8-P301L mice, suggesting that the reduction in specific force is not likely due to any problems with calcium handling/excitation contraction coupling (Fig. 4B).

We also determined specific force for the EDL muscle from AAV8-P301L tau males as the EDL muscle is distinct to the soleus muscle in that it is not a postural muscle and has limited recruitment during movement. We found that specific force was not significantly different in the AAV8-P301L vs. control males (Fig. 4C). Reflecting the soleus, the force frequency curves were similar, indicating normal calcium handling (Fig. 4D). Since the soleus muscle has a much more frequent pattern of use compared to the EDL muscle, the reduction in muscle specific force in the soleus may be linked to the pattern of its use and neural recruitment. At the time of the muscle collections for ex vivo assessment, reduced body weight was maintained at 15 months in AAV8-P301L males (Fig. 4E).

Since the tauopathy model is generated with an exogenous ICV injection of AAV8-P301L tau, the decrease in specific force of the soleus muscle could have been due to an accumulation of human tau in the soleus. This could sterically impact normal sarcomeric structure or protein–protein interactions (i.e., actin-myosin), and limit myofiber force production. Therefore we perfomed PCR for human tau and found that it was only expressed in the brain, and not in muscle tissue (Supplementary Fig. 4). Accordingly, accumulation of human tau or phosphorylated tau was not detected in the soleus of AAV8-P301L tau expressing mice (Supplementary Fig. 4B, C, E, G, H). Murine tau quantity was also unchanged in the soleus of AAV8-P301L mice (Supplementary Fig. 4D, F, G, H).

Discussion

We identified skeletal muscle abnormalities in the AAV8-P301L tauopathy mouse model as an addition to the growing evidence of skeletal muscle irregularities as peripheral symptoms of tauopathy [20–21,27]. This work is the first to emphasize skeletal muscle anomalies due to brain-specific overexpression of P301L tau inducing tauopathy.

The AAV8-P301L tau model is ideal to study muscle weakness in tauopathy because P301L tau is introduced via ICV injection under the human synapsin 1 promoter packaged in recombinant AAV8, and therefore is not endogenously overexpressed in skeletal muscle fibers (Supplementary Fig. 4). Overexpression of mutant tau in skeletal muscle could be an unintentional consequence of tauopathy models under the mouse prion promoter [23–24,29]. In the AAV8-P301L model, *in vivo* weakness is observed prior to reported cognitive deficits of the model, which aligns with the reduction in plantar flexor torque production in the 5xFAD model prior to cognitive decline and the clinical increased risk for dementia in humans with low handgrip strength [17,30–34]. Furthermore, human tau overexpression is not detected in muscle tissue and *ex vivo* muscle contractile weakness was detected with a measurement that is independent of motor neuron signaling (Fig. 4 and Supplementary Fig. 4). These findings warrant additional studies that can be leveraged using the AAV8-P301L model.

The deficit on the grip strength observed in AAV8-P301L tau-expressing mice merited investigation into skeletal muscle properties that may underpin this finding. We observed abnormalities such as mononuclear cell infiltration in H&E-stained muscle cross sections that could have been specific to the cross-section or throughout the length of the muscle. Therefore, we performed spatial transcriptomic sequencing to identify the nature of the cellular proliferative process in the fibers themselves that was not apparent in the H&E-stained sections. We observed sex specific transcriptional changes in the myofibers of AAV8-P301L tauopathy mice that change when near muscle features that make myofibers susceptible to circulating or propagating tau, such as blood vessels and nerve bundles, respectively. This finding suggests that tau has the potential to transcriptionally impact other organs beyond the central and peripheral nervous systems, and that mechanism may be mediated by proximity to circulatory or nervous systems [35].

The transcriptional environment was different in myofibers of AAV8-P301L tau expressing mice. The transcript *Amd1* was significantly differentially expressed in 5 out of 6 region types analyzed. This metabolic polyamine biosynthesis enzyme and its pathway contribute to skeletal muscle force generation, although it is not clear to what extent [36–37]. Transcriptional detection of spermine oxidase (*Smox*), also involved in polyamine biosynthesis, was differentially expressed in AAV8-P301L male myofibers proximal to nerve bundles, suggesting that the polyamine biosynthesis pathway may be altered. The consistent differential expression of *Amd1* makes the gene attractive as a biomarker. Furthermore, genes encoding proteins essential for generating force such as *Ache*, *Myh4*, and *Casq2* were altered. The upregulation of *Ache* links contractile weakness to motor neuron signaling, which should be studied in the AAV8-P301L model. Interestingly the acetylcholinesterase inhibitor Donepezil not only slows cognitive rate of decline in AD patients, but has recently been shown to improve the skeletal muscle mitochondrial respiration deficit in patients with MCI [38]. Our findings that *Ache* is upregulated suggest an acetylcholinesterase inhibitor may improve skeletal muscle outcomes. The upregulation of *Casq2* (1.18 Log2Fold Change) in AAV8-P301L males suggests compensation ensuring proper calcium buffering (as observed in the

force frequency curves from the soleus and EDL). It is unclear if the transcriptional changes represent adaptive or pathologic responses, but the observed transcriptional changes suggest that skeletal muscle force production could be impacted.

In vivo weakness, mononuclear cell infiltration displacing contractile material, and transcriptional alterations alluded to the possibility that the muscle contractile machinery in AAV8-P301L tau mice was impacted. A reasonable explanation for muscle weakness is that tauopathy affects muscle innervation, thereby influencing force production. To independently study alterations in the contractile material of the muscle, we report specific force. Since the muscle tissue is externally stimulated *ex vivo*, deficits in this measure are independent of motor neuron signaling and suggest disruption of the contractile proteins and/or increased contribution of non-muscle cells to the muscle tissue. In this study we discovered reduced specific force in the soleus muscle of AAV8-P301L tau males. This finding supports that tauopathy has peripheral consequences beyond gene expression that have detrimental outcomes to skeletal muscle funciton. Recently, reduced plantar flexor torque in the 5xFAD model was revealed by tibial nerve stimulation but not direct muscle stimulation [34]. We show that in skeletal muscle alone, independent of nerve stimulation, force production is blunted in the AAV8-P301L model. Therefore, limitations in muscle force generation may contribute to reductions in plantar flexor torque.

We did not observe a deficit in specific force of the EDL. This could be explained by the normal heterogeneity in skeletal muscle. The soleus is a mixed fiber type muscle located in the posterior of the lower hindlimb and regularly recruited for posture and movement. The EDL is primarily a fast fiber type muscle located in the anterior region of the hindlimb, does not contribute to weight-bearing activity, and is infrequently recruited. Therefore, individual muscles may be impacted by tauopathy in a distinct manner and may be important to consider in clinical cases. This finding may be underpinned by differences in muscle usage since walking requires increased soleus functional demand relative to EDL function [39–41]. AAV8-P301L tau mice have increased activity detected by IR cage sensors, and the soleus may be susceptible to chronic over-usage if the increase in IR beam break activity correlates to walking and muscle usage. Our findings may also reflect the differences in susceptibility to aging phenotypes between the two muscles [42]. The mice utilized in this study were collected at 15 months, and are not considered aged, but the tauopathy may induce aging phenotypes. Our findings may enable further studies on muscle targets underlying sarcopenic presentations in aging patients with tauopathy. Our data did not suggest a reduction in muscle size, although it may occur if the mice were allowed to age longer.

Beyond executing movement, skeletal muscle has essential roles in whole-body metabolism [43–45]. In tauopathy, it is unknown whether these functions are preserved in skeletal muscle. We observed consistent male-specific decreases in creatine kinase expression, indicating that high energy phosphate metabolism could be impacted. This supports claims that muscle metabolism is altered in tauopathy. Additionally, skeletal muscle is a primary site for glucose uptake/storage/release, and therefore significantly contributes to whole body metabolism. We observed a significant increase in *Ldha* expression in AAV8-P301L females, encoding lactate dehydrogenase A, a subunit of lactate dehydrogenase in skeletal muscle. This alludes to the preferential shift to anaerobic glycolysis and altered glucose utilization, or to the preferential production of lactate. Lactate transport has been postulated to exist from muscle fibers into circulation, and to neurons. This is enabled by monocarboxylate transporters that facilitate blood–brain barrier transport to allow lactate mediated oxidative metabolism as energy supply for the brain [46–49]. This may be a meaningful consideration when there is high metabolic stress on neurons due to NFT accumulation. Brain metabolic stress mechanisms have been described in tauopathy, such insulin signaling, inflammation, and ER stress [8–9,50–52]. These stressors may call for increased metabolic demand on skeletal muscle to preserve homeostasis.

Conclusion

Pathological tau species such as NFTs likely have far-reaching consequences in addition to neurodegeneration; our findings emphasize this in skeletal muscle. Tauopathy induces peripheral symptoms in the AAV8-P301L model and has the potential to influence additional skeletal muscle functions beyond generating force. Transcriptomic analyses indicate the potential for muscle-based biomarkers in assessing tauopathy risk, therefore positioning skeletal muscle as a source for tauopathy biomarkers in addition to blood-based biomarkers and imaging. Mechanisms underpinning reductions in force or mediating tau pathogenesis in distal muscles remain elusive and require additional efforts to understand how pathological tau mediates skeletal muscle anomalies, and the additional consequences imposed on skeletal muscle.

Methods

Mice

All animal studies were approved by the University of Florida Institutional Animal Care and Use and Committee and recombinant DNA use was approved by University of Florida EH&S Office. C57BL/6J mice were used in this study and did not have any notable physical abnormalities. Mice were maintained on food and water ad libitum and on a 12-h light/dark cycle. All mice were anesthetized and euthanized following IACUC-approved protocol at 15 months, and no physical abnormalities were detected. Brains were immediately collected and cut at the midsagittal plane, with one hemisphere fixed in 10 % formalin and the other dissected to isolate cortical and hippocampal regions before being flash frozen in liquid nitrogen. Concurrently, the tibialis anterior, gastrocnemius, and soleus were collected and flash frozen. The contralateral tibialis anterior muscle was embedded in O.C.T. compound (Tissue-Tek 4583, Sakura Finetek USA, Inc.) and frozen in liquid nitrogen-cooled isopentane for cryo-sectioning. A cohort of AAV8-P301L tau expressing mice (N = 7 males) and control mice (N = 3 males) were anesthetized and euthanized at the Physiological Assessment Core at the University of Florida, in which under anesthesia the extensor digitorum longus (EDL) and soleus muscles were carefully dissected out for mechanical testing prior to collecting the brain or other muscles.

AAV Injections

Recombinant AAV was produced and injected bilaterally into the ventricles of all neonatal mice (PND 0) as previously described [53]. The construct expressing P301L-tau under the control of the human synapsin promoter was packaged in capsid serotype 8 for this study. Control mice were injected with either an empty AAV vector packaged in serotype 8, or with a construct expressing yellow fluorescent protein under the control of the human synapsin promoter packaged in serotype 8. All animals were bilaterally injected with 2 μL (1 x 10^{13} viral genomes) of AAV8 in each hemisphere.

Grip strength and activity measures

Body weight of each mouse was measured and recorded at the time of the grip strength test. Forelimb grip strength was measured at 3 months of age following the TREAT-NMD SOP: DMD_M.2.2.001. Forelimb grip strength was measured 5 times with one minute rest periods in between. The average of the measures was used as the raw grip strength. Raw grip strength was then divided by body weight to calculate the grip strength normalized to body weight. Voluntary locomotor activity in the cage was continuously monitored using passive infrared motion detectors (Aurora; Ademco®) and the ClockLab analysis software (Actimetrics) in one-minute bins over 10 days. Locomotor activity data collected during the first two days were excluded to limit the detection of non-representative changes in activity from acclimation to a new cage.

Muscle function measures

Under anesthesia, the EDL and soleus muscles were carefully dissected out at the Physiological Assessment Core at the University of Florida Wellstone/Myology Institute, and mechanical measurements (isometric tetanic force, force/frequency relationship, muscle weight) were performed following the TREAT-NMD SOP: DMD_M.1.2.002, as described previously [54].

Immunohistochemistry and histology

15-month-old hemibrains were fixed in 10 % formalin overnight in 4 °C upon dissection. Hemibrains were embedded in paraffin and serial sections (10 μm) were cut from the midline. Immunohistochemistry (IHC) was performed as previously described [55], using the HT7 primary antibody (Thermo Fisher Scientific MN1000; 1:1000) and the corresponding Goat Anti-Mouse IgG (H + L) biotinylated secondary antibody (Vector Laboratories; 1:1000) to detect injected human derived tau with DAB labeling. The slides were imaged with the Aperio slide scanner (20x objective lens, Scan Scope™ XT, Aperio Technologies, Inc. Vista, CA).

Tibialis anterior muscles embedded in OCT compound were cryo-sectioned into 8 μm thick cross sections. General myofiber morphology was visualized by staining the sections with hematoxylin and eosin and then imaged with the Aperio slide scanner (20x or 40x objective lens, Scan Scope™ XT, Aperio Technologies, Inc. Vista, CA). After myofiber morphology was visualized, corresponding serial sections were chosen for additional IHC to demarcate myofiber perimeter. Cryo-sections were.

incubated for 1 h in blocking buffer (5 % Bovine Serum Albumin; 10 % Normal Goat Serum; 1 % Glycine; 0.1 % Triton X-100; in TBS) and then labeled with anti-laminin antibody (Millipore Sigma L9393, 1:100) to demarcate myofiber perimeter diluted in blocking buffer and incubated overnight at 4 °C. Following overnight incubation, sections were washed three times for 10 min each in blocking buffer. Corresponding secondary antibodies (ThermoFisher A-11012, Alexa Fluor™ 594) were diluted in blocking buffer for 2 h (1:500) and then washed 3 times for 10 min in blocking buffer. Immunofluorescent images were acquired and stitched automatically with the Keyence BZ-X710. Images with laminin stains were automatically processed using MyoVision 2.0 software to acquire fiber cross sectional area and minimum feret diameter as previously described [56].

Biochemical fractionation of mouse brains and western blotting

Cortical brain regions isolated from a hemibrain, that were quickly frozen in liquid nitrogen and stored at −80 °C were used for biochemical analysis. Each cortical sample was weighed and homogenized in ten volumes (10x the weight) of homogenizing buffer (50 mM tris base, 10 % glycerol, 2 % SDS, 2 % 2-mercaptoethanol, pH 8.8, protease and phosphatase inhibitors) with a Dounce homogenizer. The homogenates were fractioned to obtain a supernatant fraction with soluble tau (S1) and a pellet with sarkosyl-insoluble tau (P3) as previously described [57]. Sarkosyl-insoluble pellets (P3) were resuspended in 50 μL of 4 x Laemmli sample buffer (Bio-Rad), separated into 10 μL aliquots, and stored at −80 °C until used for western blot analysis.

Soleus tissue lysates were obtained by homogenizing the tissue in 50 volumes (50x the weight) of homogenizing buffer with a Dounce homogenizer. Samples were heated at 80 °C for 5 min and were centrifuged for 15 min at 20,000g to remove cellular debris. The supernatant was collected and stored at −80 °C until used for western blot analysis. A Bicinchoninic acid protein assay was performed on the S1 brain samples and soleus supernatant. 10 ug of protein from cortical samples and 45ug of muscle samples were diluted in 4x Laemmli sample buffer (Bio-Rad). P3 brain samples were already directly resuspended in 4x Laemmli sample buffer. All samples were heat-denatured for 5 min at 100 °C and run on a 4–20 % Criterion Tris-HCl Protein gel and transferred to PVDF membrane (Millipore). Membranes with muscle tissue homogenates were blocked in 5 % non-fat dry milk in TBS/0.2 % Triton X-100 and incubated overnight in Tau12 (Millipore Sigma; 1:1000) and actin primary antibody (Millipore Sigma; 1:1000) diluted in 5 % milk in TBS/0.1 % Triton X-100 rocking at 4 °C. Membranes were incubated in Goat-Anti-Mouse HRP-conjugated secondary antibody (SouthernBiotech; 1:2000) for 1 h at room temperature and detected by ECL (PerkinElmer). Membranes with cortical samples were

blocked in Intercept (TBS) blocking buffer (LI-COR) rocking overnight at 4 °C, and incubated for 1 h in either Tau12 (Millipore Sigma MAB2241; 1:1000), Tau46 (Santa Cruz Biotechnology Inc. sc-32274; 1:1000), H-150 (Santa Cruz Biotechnology Inc. sc-5587; 1:1000), PHF-1 (1:1000), or AT8 primary antibody (Thermo Fisher Scientific MN1020; 1:1000) diluted in TBS/0.2 % Tween-20. Membranes were incubated with the corresponding Goat Anti-Mouse IgG (H + L) IRDye secondary antibody (LI-COR 926–32212; 1:12,500) for 1 h at room temperature and imaged on an Odyssey M Imager (LI-COR).

RNA Isolation and NanoString Mouse Whole Transcriptome Atlas (WTA) assay

In order to determine the RNA integrity number (RIN) for each sample, RNA was isolated from flash frozen 8 μm thick sections of tibialis anterior muscles embedded in OCT using the RNeasy Mini Kit (Qiagen) and evaluated using the RNA high sensitivity kit (Agilent RNA 6000 Pico Kit) and an Agilent 2100 Bioanalyzer. Only samples with a RIN > 7.6 were chosen for the Nanostring Mouse Whole Transcriptome Atlas (WTA). The mouse WTA assay (NanoString Technologies) was performed as previously described [58] following the manufacturers protocol and NanoString University supplemental protocols with slides containing 8 μm thick OCT cryosections of the tibialis anterior muscle. A primary-conjugated anti-laminin antibody (Novus, 1:500) and SYTO13 (NanoString Nuclear Stain Morphology kit) were used as morphology markers. For each of the 4 groups (tauopathy male or female and control male or female), 3 biological replicates of the cross sections were used. From each cross section (12 cross sections total), regions were chosen. 3 region types were chosen (standard fibers, regions of fibers proximal to nerve bundles, and regions of fibers proximal to vasculature) on each cross section. 1–2 replicates of each region type was chosen by the user, depending on the frequency of certain muscle hallmarks in the section (regions with blood vessels or nerve bundles all had minimum one region). Every selected region was $\sim 9000\ \mu m^2$ in area. After collection of ROIs, libraries were prepared as described in protocol and submitted for sequencing to the UF Interdisciplinary Center for Biotechnology Research. FASTQ files were then converted into DCC files using BaseSpace and analyzed using the Nanostring Data Analysis suite.

Statistical analysis

GraphPad Prism 9 software was used to perform statistical tests. Results are reported as means ± standard error of the means. Unpaired Student's t-tests were performed for comparisons between AAV8-P301L tau expressing mice and controls of the same sex and of the same parameter. A two-way ANOVA was used to make multiple comparisons between tauopathy mice and controls of both sexes. $P < 0.05$ was considered significant.

Data from the NanoString Mouse Whole Transcriptome Atlas assay was analyzed on the GeoMx DSP analysis suite (NanoString). A linear mixed model with Benjamini-Hochberg correction was performed to acquire unadjusted and adjusted p-values. Targets were considered of interest with either an adjusted P value, $Q < 0.05$, $Q < 0.1$, or an unadjusted P-value < 0.05 and a Log2Fold Change of +/-1.

Lead contact:

Additional information and requests for resources should be directed to and will be fulfilled by the lead contact, Jose Abisambra (j.abisambra@ufl.edu).

Materials availability:

This study did not generate novel reagents.

CRediT authorship contribution statement

Bryan Alava: Writing – review & editing, Writing – original draft, Visualization, Validation, Methodology, Investigation, Formal analysis, Data curation, Conceptualization. **Gabriela Hery:** Writing – review & editing, Methodology, Investigation. **Silvana Sidhom:** Methodology. **Miguel Gutierrez-Monreal:** Data curation, Investigation, Software. **Stefan Prokop:** Resources. **Karyn A. Esser:** Writing – review & editing, Supervision, Resources, Funding acquisition, Conceptualization. **Jose Abisambra:** Writing – review & editing, Supervision, Resources, Funding acquisition, Conceptualization.

Declaration of competing interest

The authors declare that they have no known competing financial interests or personal relationships that could have appeared to influence the work reported in this paper.

Acknowledgements

We thank the Abisambra and Esser laboratories for the helpful discussions and training. We also thank Dr. Todd Golde and Danny Ryu for their contribution of AAV constructs. We also thank the Physiological Assessment Core and Systems Physiology and Multi-–Omics Resource Core at the University fo Florida for their support. This work was supported by NIH/NIA, United States U01AG055137-S1 (K.E.), NIH/NIAMS, United States R01AR079220 (K.E.), NIH/NIA, United States R01AG074584-02 (J.A.), NIH/NIA, United States R01AG075900-01 (J.A.), and Alzheimer's Association, United States AARG-D-21-847204 (J.A.).

Appendix A. Supplementary data

Supplementary data to this article can be found online at https://doi.org/10.1016/j.nbas.2024.100110.

References

[1] Cook C, et al. Tau deposition drives neuropathological, inflammatory and behavioral abnormalities independently of neuronal loss in a novel mouse model. Hum Mol Genet 2015. https://doi.org/10.1093/hmg/ddv336.
[2] Johnson GVW, Stoothoff WH. Tau phosphorylation in neuronal cell function and dysfunction. *J Cell Sci* Preprint at 2004. https://doi.org/10.1242/jcs.01558.
[3] Chong FP, Ng KY, Koh RY, Chye SM. Tau Proteins and Tauopathies in Alzheimer's Disease. *Cell Mol Neurobiol* Preprint at 2018. https://doi.org/10.1007/s10571-017-0574-1.
[4] Williams DR. Tauopathies: Classification and clinical update on neurodegenerative diseases associated with microtubule-associated protein tau. *Intern Med J* Preprint at 2006. https://doi.org/10.1111/j.1445-5994.2006.01153.x.
[5] Lasagna-Reeves CA, et al. Identification of oligomers at early stages of tau aggregation in Alzheimer's disease. FASEB J 2012;26:1946–59.
[6] Barbier P, et al. Role of Tau as a Microtubule-Associated Protein: Structural and Functional Aspects. Front Aging Neurosci 2019;11.
[7] Neve RL, Harris P, Kosik KS, Kurnit DM, Donlon TA. Identification of cDNA clones for the human microtubule-associated protein tau and chromosomal localization of the genes for tau and microtubule-associated protein 2. Mol Brain Res 1986;1:271–80.
[8] Meier S, et al. Pathological Tau Promotes Neuronal Damage by Impairing Ribosomal Function and Decreasing Protein Synthesis. J Neurosci 2016;36:1001.
[9] Abisambra JF, et al. Tau Accumulation Activates the Unfolded Protein Response by Impairing Endoplasmic Reticulum-Associated Degradation. The Journal of Neuroscience 2013;33:9498.
[10] Hsieh Y-C, et al. Tau-Mediated Disruption of the Spliceosome Triggers Cryptic RNA Splicing and Neurodegeneration in Alzheimer's Disease. Cell Rep 2019;29:301–316.e10.
[11] Tracy TE, et al. Tau interactome maps synaptic and mitochondrial processes associated with neurodegeneration. Cell 2022;185:712–728.e14.
[12] Jiang L, et al. Interaction of tau with HNRNPA2B1 and N6-methyladenosine RNA mediates the progression of tauopathy. Mol Cell 2021;81:4209–4227.e12.
[13] Gustke N, Trinczek B, Biernat J, Mandelkow E-M, Mandelkow E. Domains of tau Protein and Interactions with Microtubules. Biochemistry 1994;33:9511–22.
[14] Maziuk BF, et al. RNA binding proteins co-localize with small tau inclusions in tauopathy. Acta Neuropathol Commun 2018;6:71.
[15] Drummond E, et al. Phosphorylated tau interactome in the human Alzheimer's disease brain. Brain 2020;143:2803–17.
[16] Meier S, et al. Identification of Novel Tau Interactions with Endoplasmic Reticulum Proteins in Alzheimer's Disease Brain. Journal of Alzheimer's Disease 2015;48:687–702.
[17] Boyle PA, Buchman AS, Wilson RS, Leurgans SE, Bennett DA. Association of Muscle Strength With the Risk of Alzheimer Disease and the Rate of Cognitive Decline in Community-Dwelling Older Persons. Arch Neurol 2009;66:1339–44.
[18] Moon Y, Moon WJ, Kim JO, Kwon KJ, Han SH. Muscle Strength Is Independently Related to Brain Atrophy in Patients with Alzheimer's Disease. Dement Geriatr Cogn Disord 2019. https://doi.org/10.1159/000500718.
[19] Burns JM, Johnson DK, Watts A, Swerdlow RH, Brooks WM. Reduced Lean Mass in Early Alzheimer Disease and Its Association With Brain Atrophy. Arch Neurol 2010;67:428–33.
[20] Xu H, et al. Age Related Changes in Muscle Mass and Force Generation in the Triple Transgenic (3xTgAD) Mouse Model of Alzheimer's Disease. Front Aging Neurosci 2022;14.
[21] Pan J-X, et al. Muscular Swedish mutant APP-to-Brain axis in the development of Alzheimer's disease. Cell Death Dis 2022;13:952.
[22] Ramsden M, et al. Age-Dependent Neurofibrillary Tangle Formation, Neuron Loss, and Memory Impairment in a Mouse Model of Human Tauopathy (P301L). The Journal of Neuroscience 2005;25:10637.
[23] Yoshiyama Y, et al. Synapse Loss and Microglial Activation Precede Tangles in a P301S Tauopathy Mouse Model. Neuron 2007;53:337–51.
[24] Lewis J, et al. Neurofibrillary tangles, amyotrophy and progressive motor disturbance in mice expressing mutant (P301L) tau protein. Nat Genet 2000;25:402–5.
[25] SantaCruz K, et al. Tau Suppression in a Neurodegenerative Mouse Model Improves Memory Function. Science 2005;1979(309):476–81.
[26] Blackmore T, et al. Tracking progressive pathological and functional decline in the rTg4510 mouse model of tauopathy. Alzheimers Res Ther 2017;9:77.
[27] Matthews I, et al. Skeletal muscle TFEB signaling promotes central nervous system function and reduces neuroinflammation during aging and neurodegenerative disease. Cell Rep 2023;42:113436.
[28] Samarra I, et al. Gender-Related Differences on Polyamine Metabolome in Liquid Biopsies by a Simple and Sensitive Two-Step Liquid-Liquid Extraction and LC-MS/MS. Biomolecules 2019;9.
[29] Smith JD, et al. Prion Protein Expression and Functional Importance in Skeletal Muscle. Antioxid Redox Signal 2011;15:2465–75.
[30] McGrath R, et al. Handgrip Strength Is Associated with Poorer Cognitive Functioning in Aging Americans. Journal of Alzheimer's Disease 2019;70:1187–96.
[31] Alfaro-Acha A, et al. Handgrip Strength and Cognitive Decline in Older Mexican Americans. The Journals of Gerontology: Series A 2006;61:859–65.
[32] Buchman AS, Wilson RS, Boyle PA, Bienias JL, Bennett DA. Grip Strength and the Risk of Incident Alzheimer's Disease. Neuroepidemiology 2007;29:66–73.
[33] Duchowny KA, et al. Associations Between Handgrip Strength and Dementia Risk, Cognition, and Neuroimaging Outcomes in the UK Biobank Cohort Study. JAMANetw Open 2022;5:e2218314–.
[34] Brisendine MH, et al. Neuromuscular dysfunction precedes cognitive impairment in a mouse model of Alzheimer's Disease. *Function* zqad066 2023. https://doi.org/10.1093/function/zqad066.
[35] Castillo-Carranza DL, et al. Cerebral microvascular accumulation of tau oligomers in Alzheimer's disease and related tauopathies. Aging Dis 2017;8:257–66.
[36] Abukhalaf IK, et al. Effect of Hindlimb Suspension and Clenbuterol Treatment on Polyamine Levels in Skeletal Muscle. Pharmacology 2002;65:145–54.
[37] Lee NKL, MacLean HE. Polyamines, androgens, and skeletal muscle hypertrophy. J Cell Physiol 2011;226:1453–60.
[38] Morris JK, et al. Mild Cognitive Impairment and Donepezil Impact Mitochondrial Respiratory Capacity in Skeletal Muscle. Function 2021;2:zqab045.
[39] Liu MQ, Anderson FC, Schwartz MH, Delp SL. Muscle contributions to support and progression over a range of walking speeds. J Biomech 2008;41:3243–52.
[40] Liu MQ, Anderson FC, Pandy MG, Delp SL. Muscles that support the body also modulate forward progression during walking. J Biomech 2006;39:2623–30.
[41] Pandy MG, Lin Y-C, Kim HJ. Muscle coordination of mediolateral balance in normal walking. J Biomech 2010;43:2055–64.
[42] Valdez G, Tapia JC, Lichtman JW, Fox MA, Sanes JR. Shared Resistance to Aging and ALS in Neuromuscular Junctions of Specific Muscles. PLoS One 2012;7:e34640-.
[43] Zurlo F, Larson K, Bogardus C, Ravussin E. Skeletal muscle metabolism is a major determinant of resting energy expenditure. J Clin Invest 1990;86:1423–7.
[44] Zurlo F, Nemeth PM, Choksi RM, Sesodia S, Ravussin E. Whole-body energy metabolism and skeletal muscle biochemical characteristics. Metabolism 1994;43:481–6.
[45] Argilés JM, Campos N, Lopez-Pedrosa JM, Rueda R, Rodriguez-Mañas L. Skeletal Muscle Regulates Metabolism via Interorgan Crosstalk: Roles in Health and Disease. J Am Med Dir Assoc 2016;17:789–96.
[46] Xue X, Liu B, Hu J, Bian X, Lou S. The potential mechanisms of lactate in mediating exercise-enhanced cognitive function: a dual role as an energy supply substrate and a signaling molecule. Nutr Metab (Lond) 2022;19:52.
[47] Pierre K, Pellerin L. Monocarboxylate transporters in the central nervous system: distribution, regulation and function. J Neurochem 2005;94:1–14.
[48] Bouzier-Sore A-K, et al. Competition between glucose and lactate as oxidative energy substrates in both neurons and astrocytes: a comparative NMR study. Eur J Neurosci 2006;24:1687–94.

[49] Bergersen LH. Lactate Transport and Signaling in the Brain: Potential Therapeutic Targets and Roles in Body—Brain Interaction. J Cereb Blood Flow Metab 2014;35:176–85.
[50] Nilson AN, et al. Tau Oligomers Associate with Inflammation in the Brain and Retina of Tauopathy Mice and in Neurodegenerative Diseases. Journal of Alzheimer's Disease 2017;55:1083–99.
[51] Gonçalves RA, Wijesekara N, Fraser PE, De Felice FG. The Link Between Tau and Insulin Signaling: Implications for Alzheimer's Disease and Other Tauopathies. Front Cell Neurosci 2019;13.
[52] Lyra e Silva NM, et al. Pro-inflammatory interleukin-6 signaling links cognitive impairments and peripheral metabolic alterations in Alzheimer's disease. *Transl.* Psychiatry 2021;11:251.
[53] Chakrabarty P, et al. Capsid Serotype and Timing of Injection Determines AAV Transduction in the Neonatal Mice Brain. PLoS One 2013;8:e67680-.
[54] AU-Moorwood C, AU - Liu M, AU - Tian Z, AU - Barton ER. Isometric and Eccentric Force Generation Assessment of Skeletal Muscles Isolated from Murine Models of Muscular Dystrophies. *JoVE* e50036 2013. https://doi.org/10.3791/50036.
[55] Sakthivel R, et al. Fixed Time-Point Analysis Reveals Repetitive Mild Traumatic Brain Injury Effects on Resting State Functional Magnetic Resonance Imaging Connectivity and Neuro-Spatial Protein Profiles. J Neurotrauma 2023. https://doi.org/10.1089/neu.2022.0464.
[56] Viggars MR, Wen Y, Peterson CA, Jarvis JC. Automated cross-sectional analysis of trained, severely atrophied, and recovering rat skeletal muscles using MyoVision 2.0. J Appl Physiol 2022;132:593–610.
[57] Sahara N, et al. Assembly of tau in transgenic animals expressing P301L tau: alteration of phosphorylation and solubility. J Neurochem 2002;83:1498–508.
[58] Zimmerman SM, et al. Spatially resolved whole transcriptome profiling in human and mouse tissue using Digital Spatial Profiling. Genome Res 2022;32:1892–905.